frontiers | Frontiers in Nuclear Engineering

TYPE Original Research
PUBLISHED 15 January 2025
DOI 10.3389/fnuen.2024.1523026

OPEN ACCESS

EDITED BY
Walter Villanueva,
Bangor University, United Kingdom

REVIEWED BY
Matteo D'Onorio,
Sapienza University of Rome, Italy
Nathalie Seiler,
Commissariat à l'Energie Atomique et aux Energies Alternatives (CEA), France
Andrei Komlev,
Royal Institute of Technology, Sweden

*CORRESPONDENCE
Yapei Zhang,
zhangyapei@xjtu.edu.cn

RECEIVED 05 November 2024
ACCEPTED 26 December 2024
PUBLISHED 15 January 2025

CITATION
Wu S, Zhang Y, Yu J, Bai J, Tian W, Qiu S and Su GH (2025) Experimental research on heat transfer characteristics of a two-layer corium pool based on a three-dimensional ellipsoidal lower plenum.
Front. Nucl. Eng. 3:1523026.
doi: 10.3389/fnuen.2024.1523026

Experimental research on heat transfer characteristics of a two-layer corium pool based on a three-dimensional ellipsoidal lower plenum

Shihao Wu, Yapei Zhang*, Jian Yu, Jingyuan Bai, Wenxi Tian, Suizheng Qiu and G. H. Su

State Key Laboratory of Multiphase Flow in Power Engineering, School of Nuclear Science and Technology, Shaanxi Engineering Research Center of Advanced Nuclear Energy, Xi'an Jiaotong University, Xi'an, China

To better understand the application of IVR (In-Vessel Retention), extensive experiments have been conducted on the heat transfer characteristics of molten pool. However, most research mainly focuses on hemispherical lower heads, and the research on ellipsoidal lower head suitable for small pressurized water reactors is relatively lacking. In order to provide some reference for the implementation of IVR with ellipsoidal lower head, this paper conducted the experimental study on the heat transfer characteristics of a three-dimensional double-layer molten pool based on the design of a small pressurized water reactor. The test section consists of two parts: ellipsoidal and cylindrical, with a span of 1150 mm and a total height of 700 mm. The molten material is simulated by nitrate mixture (20mol%$NaNO_3$-80mol%KNO_3), and electric heating wire is chosen to simulate the oxide layer decay heat. The effects of heating power, oxide layer height and layered partition thickness on heat transfer characteristics of two-layer molten pool under static conditions were studied. The results show that the thermal stratification phenomenon mainly occurs in the lower and middle regions of the oxide layer, with a smaller dimensionless temperature gradient in the upper region; with the similar volumetric power densities, the height of the oxide layer has little effect on the wall heat flux density; the layered partition increases the thermal resistance between the two layers and reduces the upward heat transfer to the ceramic pool. In addition, the heat transfer relationships in the oxide layer, both downward and upward, are fitted for the internal Rayleigh number range of 3.43×10^{12} to 1.54×10^{13}.

KEYWORDS

severe accident, two-layer, corium pool, IVR, ellipsoidal

1 Introduction

In the history of peaceful use of nuclear energy, there have been three major nuclear power plant accidents, namely, the Three Mile Island accident (Wolf et al., 1994), the Chernobyl accident (Tuttle and Becker, 2000) and the Fukushima accident (Younghwan et al., 2013). These three nuclear accidents have made people deeply aware of the great risks and challenges after severe accidents in nuclear power plants. Especially, as happened in the

Three Mile Island accident in 1979, if the heat generated in the reactor cannot be taken away quickly and effectively in accident, the temperature in the reactor will rise rapidly. When the reactor core melts, the high-temperature molten material will relocate to the lower plenum of pressure vessel, forming a corium pool. Moreover, heat will be generated continuously due to decay, which will be a serious threat to the integrity of reactor pressure vessel (Ma, 2012; Rempe et al., 2008).

Therefore, in-vessel retention (IVR), which adopts different methods to retain the molten material in the lower head to maintain the integrity of the pressure vessel, has been considered as one of the most important management strategies for severe reactor accidents (Zhang et al., 2013). External reactor vessel cooling (ERVC) technology achieves the external cooling of the pressure vessel by injecting water into the reactor cavity to submerge the lower head of the pressure vessel (Henry and Fauske, 1993; Zhang et al., 2013; Rempe et al., 1998). IVR-ERVC technology has been applied to AP600 and AP1000 designed in the United States, APR1400 developed in Korea and HPR1000 and CAP1400 developed in China (Ma et al., 2016).

In the past decades, a large number of experiments on heat transfer characteristics of molten pool have been carried out based on IVR-ERVC, such as BALI (Bonnet, 1999), SIMECO (Theerthan et al., 2001), COPO (Kymäläinen et al., 1994), RASPLAV (Asmolov et al., 2001), ACOPO (Theofanous et al., 1997), LIVE (Gaus-Liu et al., 2010), COPRA (Zhang et al., 2016a; Zhang et al., 2016b; Luo et al., 2018), and MORN experiment (Chen et al., 2018), etc. In addition, the aluminum sheet was arranged in the experimental section of COPO experiment (Helle et al., 1999), which not only realized the physical stratification of the molten pool, but also simulated the oxide crust between the two layers. The upward Nu_{up} and sideward Nu_{sd} obtained from COPO experiment were similar to the Globe-Dropkin and Churchill-Chu correlations, respectively. In SIMECO experiment (Theerthan et al., 2001), it was found that the interface produces additional resistance to the upward heat transfer, and the maximum heat load of pressure vessel appears below the interface. Similarly, LIVE-3D (Miassoedov et al., 2014) adopted a copper plate to realize the stratification of the molten pool, and the experiment on the heat transfer characteristics of the two-layer molten pool was carried out. The results showed that the maximum temperature of the molten pool and the maximum wall heat flux both appear below the copper plate. Recently, with stainless steel plate selected as layered partition, COPRA experiment (Zhou et al., 2020) was carried out based on COPRA facility. And the downward heat transfer Nu_{dn} and the upward heat transfer Nu_{up} obtained from COPRA experiment were in accordance with the previous data or empirical correlations.

It should be noted that the most studies carried out are based on the hemisphere-shaped lower head, while there are few researches on ellipsoidal lower head. Thus, experimental study on heat transfer characteristics of two-layer corium pool based on three-dimensional ellipsoidal lower plenum was carried out. This work helps to better understand the heat transfer characteristics of two-layer molten pool, which is beneficial for the design and analysis of IVR.

2 Experimental program

2.1 Overview of the test facility

As schematically shown in Figure 1, the three-dimensional ellipsoidal test section (COPRA-ROC) is composed of an ellipsoidal lower head, a cylinder, an upper cover plate, a layered partition and a cooling channel. The ellipsoidal lower head, whose inner diameter and depth are 1,150 mm and 286 mm respectively, is welded with cylinder. A layered partition made of stainless steel with a thickness of 20 mm or 30 mm is placed in the test section to simulate the stratified corium pools. The heating wires are arranged in the lower part to simulate the homogenously decay heat in the lower oxide layer, while no heat is generated in the upper metal layer. An approximately isothermal cooling boundary condition is offered by the cooling channel, whose outer wall is welded with the upper cylinder to form a shell cooling path with a width of 120 mm. An adiabatic boundary condition is adopted to the top wall. Cylindrical openings with a diameter of 60 mm are designed in the top lid and layered partition for the injection or discharge of the molten salt. Furthermore, the same cylindrical openings are designed in the middle of two plates as the outlet of fixed bracket.

As mentioned above, five layers of spiral heating wires are evenly installed in the test section to simulate the homogeneous decay heat generated within the oxide layer. The test section is divided into six areas by the five layers of heating wire, as shown in Figure 2. In the height direction, the distance between adjacent heating wires is 80mm, and the bottom heating wire is 40 mm from the bottom of the test section. In order to avoid affecting the temperature distribution on the wall of the molten pool, the minimum distance between the heating wire and the inner wall of the pressure vessel should be greater than 50 mm. The heating wire with a diameter of 6 mm can provide a maximum heating power of 4 kW, and the total power of the test section is 20 kW. The heating power of heating wire can be adjusted continuously according to different experimental conditions. Before each experiment, the power of each layer of electric heating wire is adjusted based on the heating volume of each layer, while maintaining a constant total heating power, to provide an approximately uniform volumetric power. The heating wires are positioned through a solid stainless steel skeleton, which is welded on the central shaft of the molten pool. For the sake of minimizing the impact on the flow field of the molten pool, the cables of heating wires are led out at the edge of the molten pool.

2.2 The parameter measurements

Inside the three-dimensional ellipsoidal test section, to obtain the temperature field inside the molten pool, thermocouples with a total number of 72 are uniformly positioned along the radial and height directions at four azimuth angles of 0°, 90°, 180° and 270°, as shown in Figure 3. The detailed positions of these thermocouples are listed in Table 1. As can be seen from Figure 4, in order to obtain the wall heat flux of the molten pool, nine groups of thermocouples are arranged on the inner and outer walls of the test section at four azimuth angles to measure the inner and outer wall temperature of the molten pool. The heat flux of ellipsoidal lower head is calculated

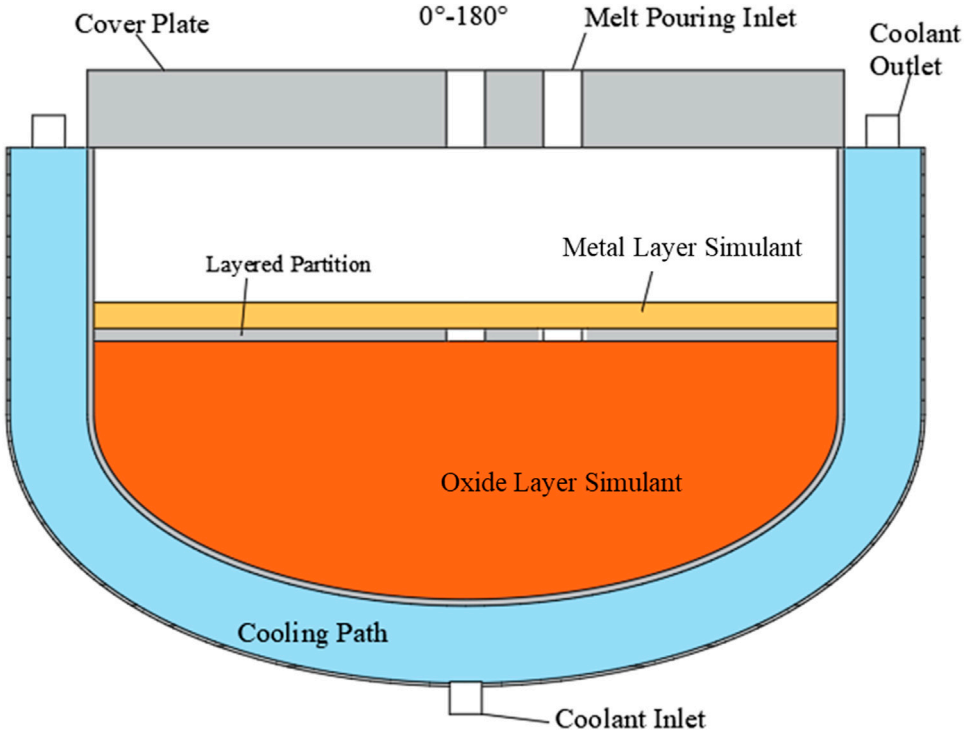

FIGURE 1
Schematic diagram of test section.

by Equation 1 and the heat flux of upper cylinder is calculated by Equation 2.

$$q = \lambda_{wall}\left(\frac{T_i - T_o}{\delta}\right) \cdot \frac{R_i}{R_o} \tag{1}$$

$$q = \frac{\lambda_{wall}}{R_o} \frac{T_i - T_o}{\ln\left(R_o/R_i\right)} \tag{2}$$

Where, R_i and R_o represent the curvature radius of the inner and outer wall of the ellipsoid and the inner and outer radius of the cylinder respectively; λ_{wall} is the thermal conductivity of wall material; T_i and T_o are the temperatures of inner wall and outer wall respectively; δ is the wall thickness.

In addition, 8 groups of thermocouples are arranged on the layered partition to measure the upper and lower surfaces temperature of the layered partition, which is used to calculate the heat flux transmitted from the lower oxide layer to the upper metal layer. The heat flux can be calculated as follows:

$$q_{partition} = -\lambda_{partition}\frac{T_{dn} - T_{up}}{\delta_{partition}}$$

Where, $\lambda_{partition}$ is thermal conductivity of layered partition; T_{dn} and T_{up} are temperatures of the lower and upper surfaces of layered partition respectively; $\delta_{partition}$ is thickness of layered partition.

In order to obtain the crust thickness of the inner wall of the test section, 12 multipoint thermocouples are arranged at four azimuth angles for calculation. The schematic diagram of multipoint thermocouples arrangement is shown in Figure 5.

In the experiment, the direct measurement parameters and their uncertainties are shown in Table 2. The direct measurement parameters include temperature parameters, height parameters, water flow rate in the coolant channel and heating power. The measuring uncertainty (U) can be calculated based on the instruments error (Δ_1) and acquisition system error (Δ_2), the equation is as follows:

$$U = \frac{\Delta_1 + \Delta_2}{\sqrt{3}}$$

2.3 Test conditions and procedures

As we know, many factors such as heating power and molten pool height will have a certain impact on the heat transfer characteristics of molten pool. In this two-layer molten pool experiment, the layered molten pool is realized by placing a layered partition in the test section. Therefore, considering the effects of different heating power, different oxide layer height and layered partition thickness, a total of 10 groups of test conditions were carried out, as shown in Table 3. In tests with different heights of oxide layers, the layered partition will be moved and rewelded.

Referring to the molten pool heat transfer experiments such as COPRA and LIVE, the binary mixture of 20 mol%$NaNO_3$–80 mol% KNO_3 is selected as the simulant material for both molten pools. The solidus temperature and liquidus temperature of mixture are 224°C and 284°C respectively. The molten nitrate mixture is injected into

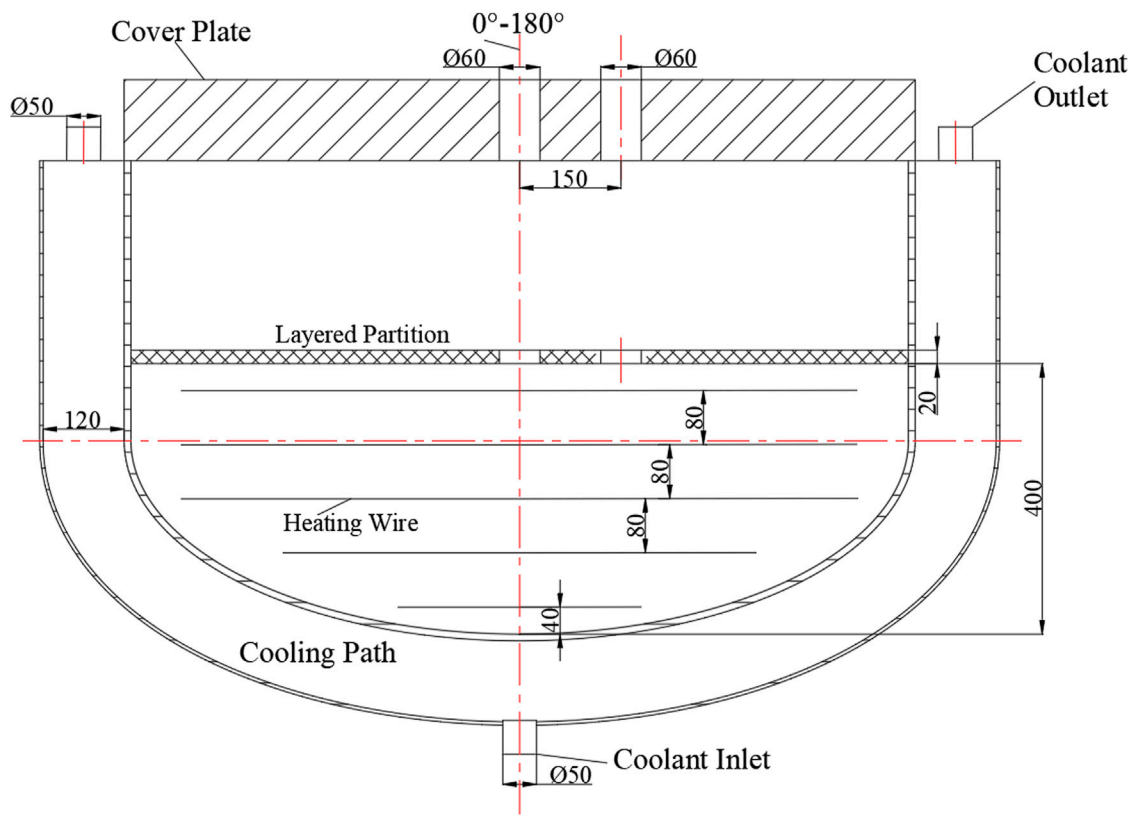

FIGURE 2
Design diagram of test section.

the test section to the required height, and the heating power is adjusted to the required power. Meanwhile, the temperature of cooling water is approximately maintained near the room temperature during the experiment. Finally, the molten pool will reach a stable state under the joint action of internal heating and external cooling, that is, the temperature of the molten pool will vary no more than 1°C for 2 h. Then, the experimental data are collected, processed and analyzed.

3 Results and discussions

In this section, the experimental results are shown and discussed in detail. Firstly, the effects of heating power, oxide layer height and layered partition thickness on the heat transfer characteristics of two-layer molten pool are discussed. Then, the downward and upward heat transfer equations of the molten pool obtained from the experiment are given.

3.1 Different effects on heat transfer characteristics of corium pool

3.1.1 Effects of heating power

Figure 6 depicts the temperature distribution of molten pool along the height direction under test 1–3 in the steady-state stage. The heating power of these tests are 12 kW, 10 kW, and 8 kW respectively. It can be seen from the figure that obvious thermal stratification occurs in the molten pool, and the peak temperature of the molten pool appears near the layered partition in the oxide layer area. However, as there is no internal heat source in the metal layer, the temperature of the molten pool decreases rapidly, and even crust may occur at the top of the molten pool.

The distribution of wall heat flux along the arc length ratio in test 1–3 is shown in the Figure 7. The wall heat flux changes little in the lower part of the oxide layer (arc length ratio is less than 0.6). Then, with the further increase of arc length ratio, the wall heat flux increases rapidly and decreases after reaching the peak near the layered partition. Higher heating power will lead to higher wall heat flux, which is similar to the effects on temperature distribution of the molten pool.

As shown in Figure 8, the distribution of crust thickness on the wall of pressure vessel under test 1–3 in the steady-state stage is given. It can be found that the thickness of crust decreases gradually with the increase of arc length ratio. The greater the heating power, the smaller the thickness of the crust. Therefore, the downward thermal resistance of the molten pool decreases and the wall heat flux increases.

3.1.2 Effects of oxide layer height

With the same partition thickness of 20 mm and metal layer height of 80 mm, the oxide layer heights for tests 2 and 9 are

10.3389/fnuen.2024.1523026

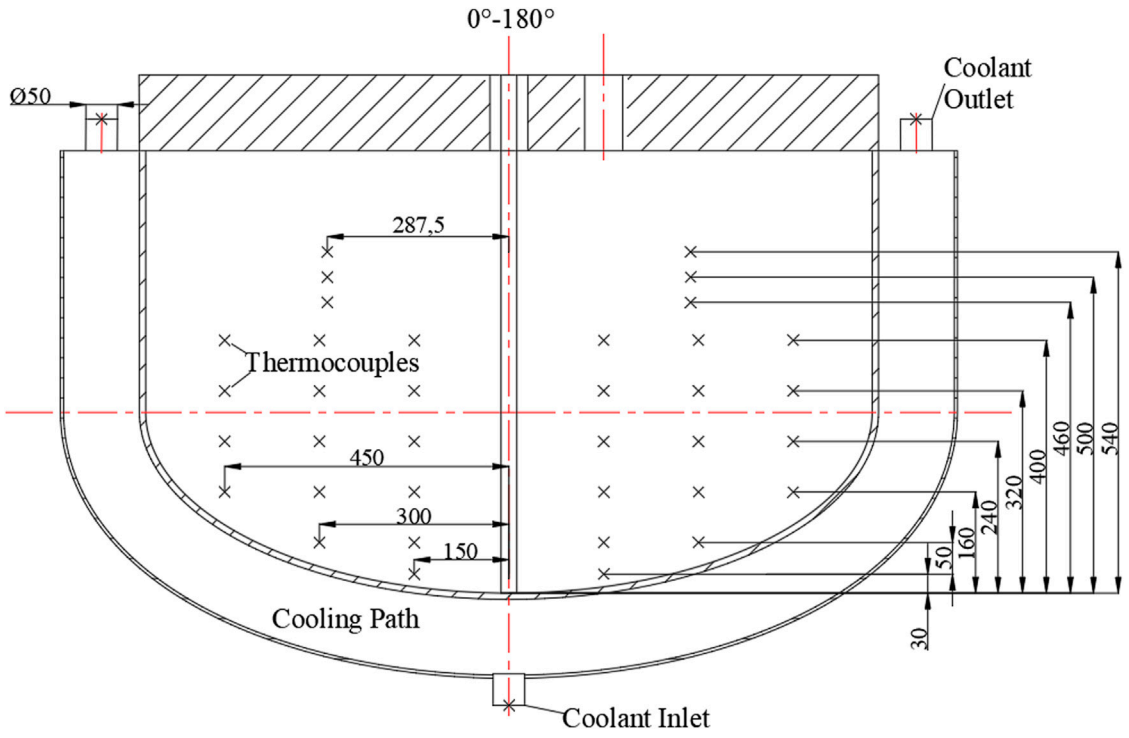

FIGURE 3
Schematic diagram of thermocouples in the test section.

TABLE 1 Positions of the thermocouples.

Thermocouple layer	Numbers	Height from bottom/mm	Distance from middle axis/mm
1	4	30	150
2	8	80	150, 300
3	12	160	150, 300, 450
4	12	240	150, 300, 450
5	12	320	150, 300, 450
6	12	400	150, 300, 450
7	4	460	287.5
8	4	500	287.5
9	4	540	287.5

400 mm and 320 mm, respectively. Moreover, in order to ignore the influence of heating power, these two tests have similar volumetric power densities. Therefore, the heating power of test 2 is 10 kW, and for test 9 is 8 kW. The temperature distribution of molten pool along the height direction in the steady-state stage under test 2 and test 9 is compared in Figure 9. It can be found that the temperature distribution of the two tests is very consistent in the oxide layer. However, the temperature at the top of the metal layer in test 2 is lower than that in test 9, which may be due to the total height of test 2 is higher and the heat transfer resistance from the metal layer to the upper cover plate is smaller. The distributions of wall heat flux and crust thickness of the two tests are shown in Figures 10, 11. Since the reduction in the oxide layer thickness is relatively small, its impact on the heat flux at the molten pool wall and crust thickness is not significant.

3.1.3 Effects of layered partition thickness

The layered partition with thickness of 20 mm and 30 mm selected as layered partition, the effect of partition thickness on heat transfer characteristics of two-layer molten pool is studied. As shown in Figure 12, the heat flux transferred downward from the

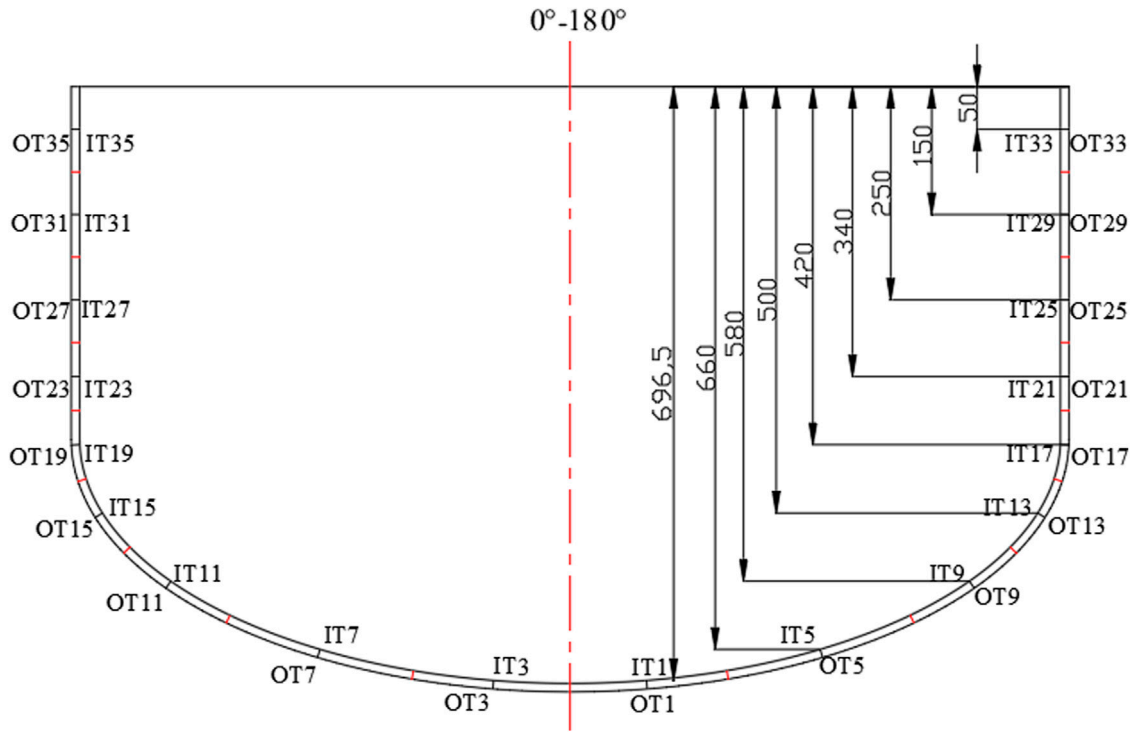

FIGURE 4
Schematic diagram of thermocouples on the wall of the test section.

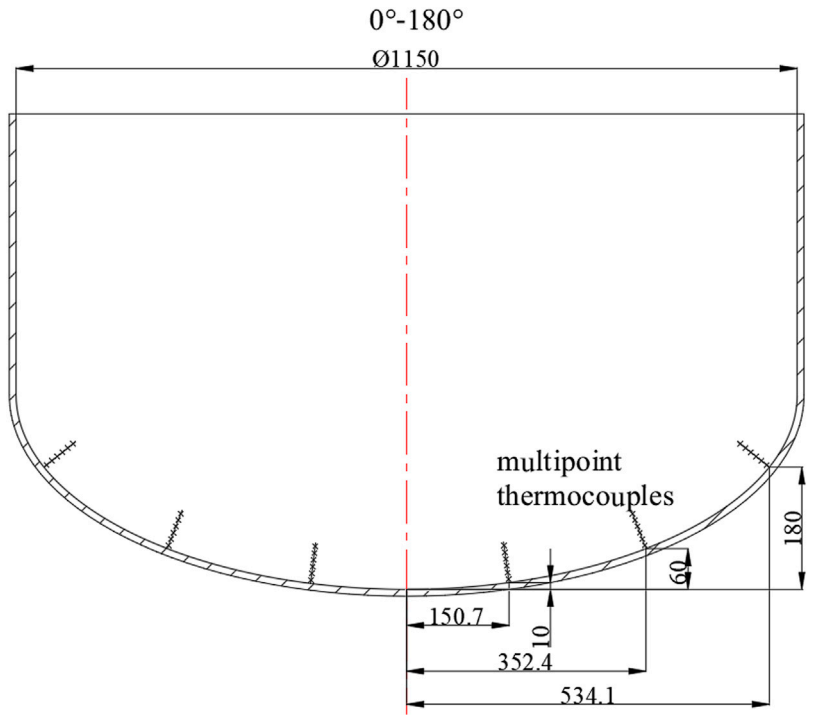

FIGURE 5
Schematic diagram of multipoint thermocouples layout.

TABLE 2 The uncertainty of directly measuring parameters.

Directly measuring parameters	Instrument	Δ_1	Δ_2	U
Temperature	K thermocouple	0.4%	0.02%	0.242%
Height	Ruler	0.01%	—	0.006%
Water flow rate	Liquid flowmeter	0.5%	0.02%	0.300%
Heating voltage	Voltage transducer	0.5%	0.02%	0.300%
Heating current	Current transducer	0.2%	0.02%	0.127%

TABLE 3 Test conditions.

Test	Oxide layer height/mm	Metal layer height/mm	Partition thickness/mm	Heating power/kW	Volumetric power/ MW·m^{-3}
1	400	80	20	12	51.5
2	400	80	20	10	42.9
3	400	80	20	8	34.3
4	400	120	30	12	51.5
5	400	120	20	12	51.5
6	400	120	20	10	42.9
7	400	120	20	8	34.3
8	320	80	20	10	31.6
9	320	80	20	8	25.3
10	320	80	20	6	19.0

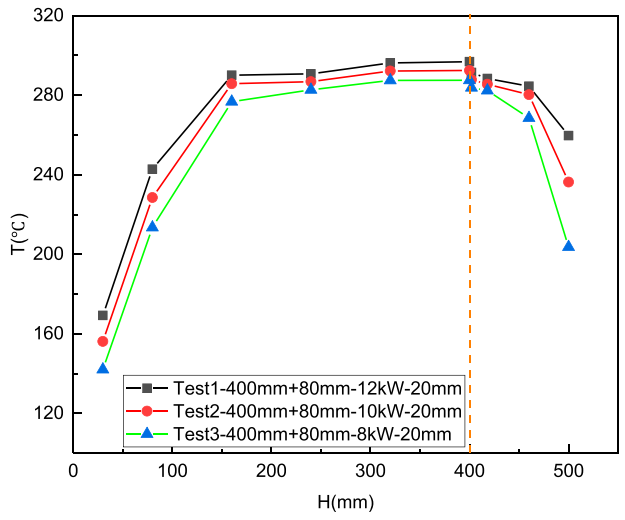

FIGURE 6
The distributions of temperature with different heating powers.

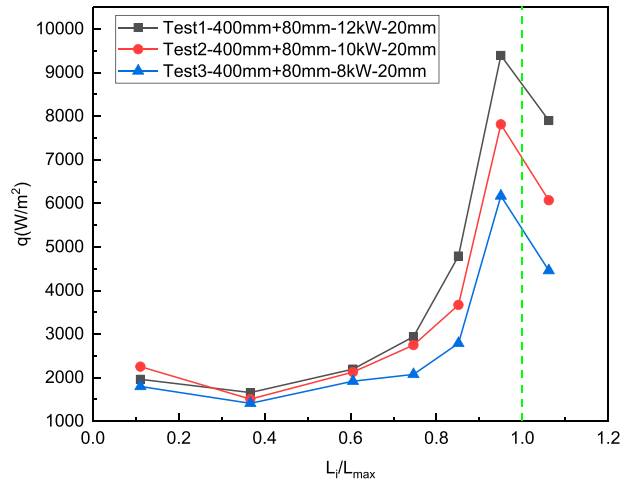

FIGURE 7
The distributions of wall heat flux with different heating powers.

oxide layer in test 4 with 30 mm partition is higher than that in test 5 with 20 mm partition.

Correspondingly, the wall crust thickness in test 5 is thicker as shown in Figure 13. It can be inferred that with the increase of the thickness of the layered partition, the heat transfer resistance from the lower oxide layer to the upper metal layer increases, resulting in increase of the downward heat transfer of the molten pool.

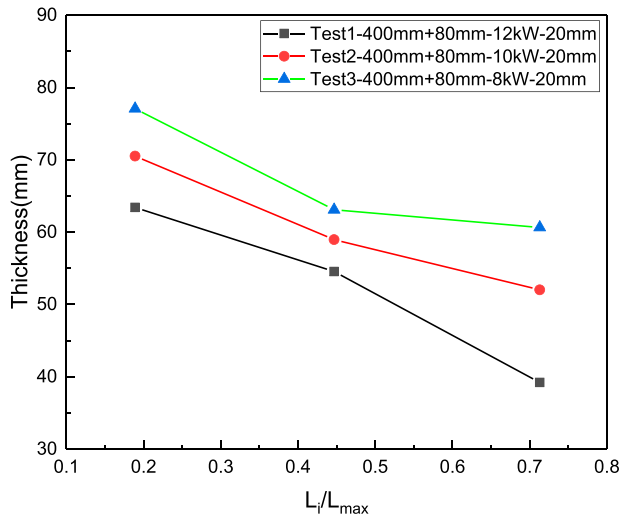

FIGURE 8
The distributions of crust thickness with different heating powers.

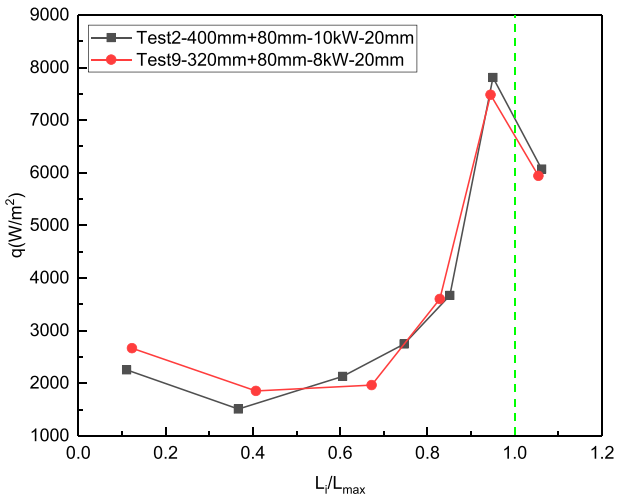

FIGURE 10
The distributions of wall heat flux with different oxide layer heights.

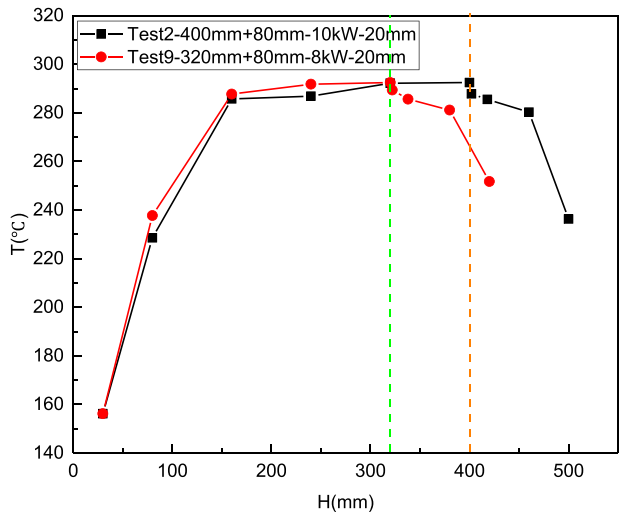

FIGURE 9
The distributions of temperature with different oxide layer heights.

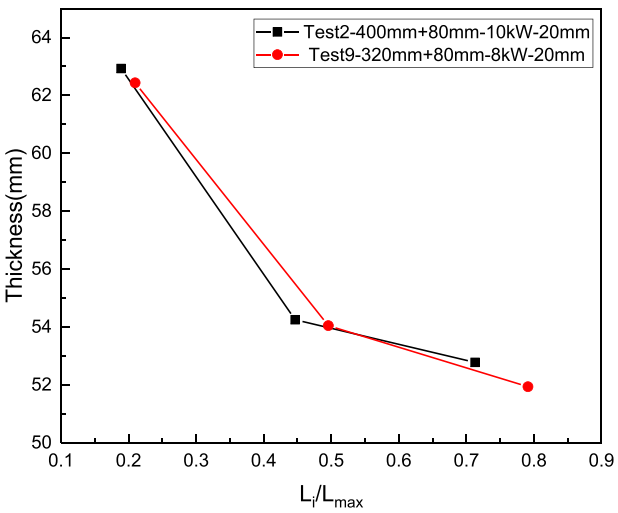

FIGURE 11
The distributions of crust thickness with different oxide layer heights.

3.2 The heat transfer characteristics of molten pool

With the temperature distributions obtained under the above 10 tests normalized, the dimensionless temperature distributions of oxide molten pool with dimensionless height are obtained, as shown in Figure 14. It can be seen from the figure that the dimensionless temperature distributions obtained from different tests are in good agreement, ignoring the effects of heating power, oxide layer height and layered partition thickness. The dimensionless temperature increases with the height of the molten pool, and the peak value is about 1.18. The relationship between dimensionless temperature and height is as follows:

$$\frac{T}{T_{ave}} = 1.162 - 0.95\exp\left(-6.185 \cdot \frac{H}{H_{\max}}\right)$$

Similarly, the wall heat flux is normalized to obtain the distribution of dimensionless heat flux with arc length ratio, as shown in Figure 15. It can be found that when the arc length ratio is less than 0.8, the dimensionless heat fluxes under different tests change little. Then, with arc length ratio increasing, the dimensionless heat fluxes increase sharply. The maximum value can reach about 2.51. The relationship between dimensionless heat flux and arc length ratio is given by:

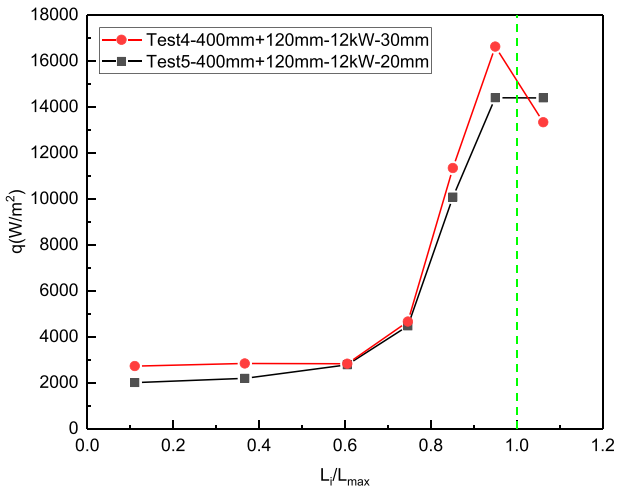

FIGURE 12
The distributions of wall heat flux with different layered partition thickness.

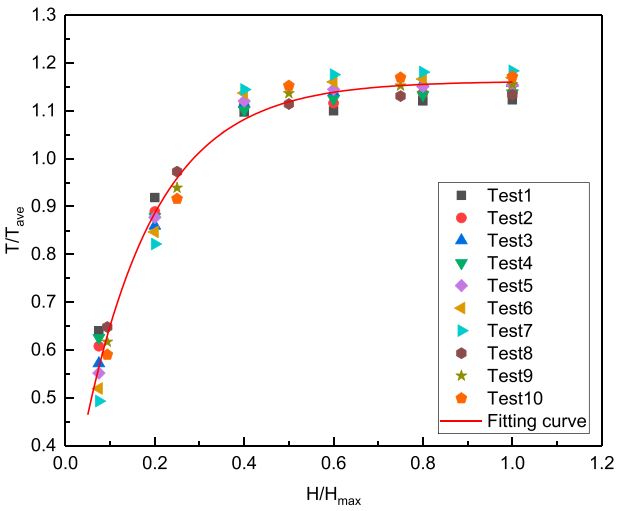

FIGURE 14
The distributions of dimensionless temperature.

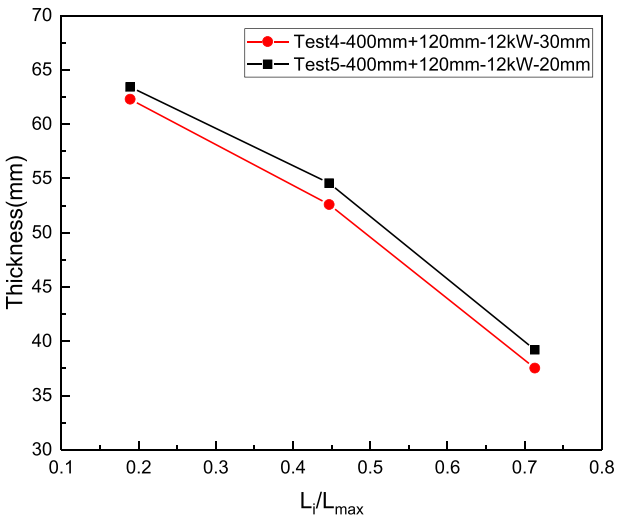

FIGURE 13
The distributions of crust thickness with different layered partition thickness.

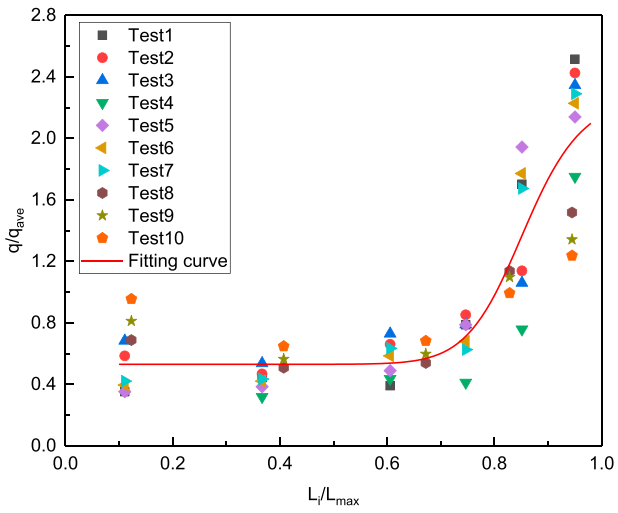

FIGURE 15
The distributions of dimensionless wall heat flux.

$$\frac{q}{q_{ave}} = 2.287 - \frac{1.753}{1 + 11.406 \cdot \left(L_i/L_{\max}\right)^{15.714}}$$

As shown in Figures 16, 17, the distributions of downward heat transfer Nu_{dn} and upward heat transfer Nu_{up} with Ra' are presented respectively. The heat transfer Nu of molten pool increases exponentially with Ra'. In the range of Ra' from 3.43×10^{12} to 1.54×10^{13}, the ranges of downward heat transfer Nu_{dn} and upward heat transfer Nu_{up} are 106.97–211.18 and 227.62–334.12, respectively. The relationships of downward heat transfer Nu_{dn} and upward heat transfer Nu_{up} with Ra' are as follows:

$$Nu_{up} = 1.669Ra'^{0.171}$$

$$Nu_{dn} = 0.011Ra'^{0.315}$$

The relationships obtained from the ACOPO experiment (Theofanous et al., 1997) are also added to in Figures 16, 17 for comparison, and its predicted values are relatively higher than the experimental values.

4 Conclusion

In this paper, a two-layer molten pool experimental system based on ellipsoidal lower plenum was built, and a series of two-layer molten pool tests under static conditions were carried out. The effects of different heating power, oxide layer height and layered

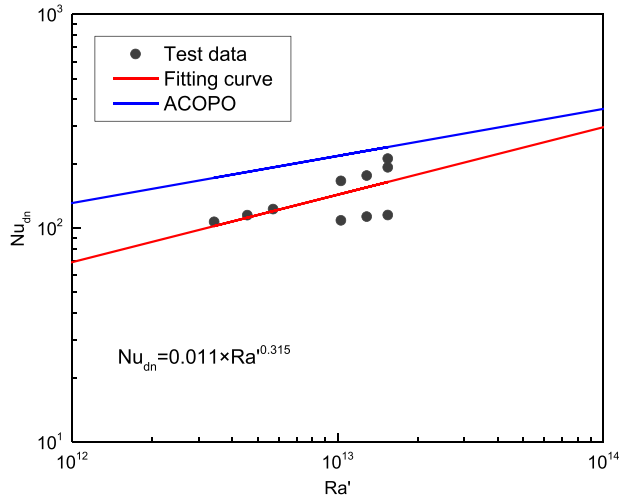

FIGURE 16
The relationship between Nu_{dn} and Ra'.

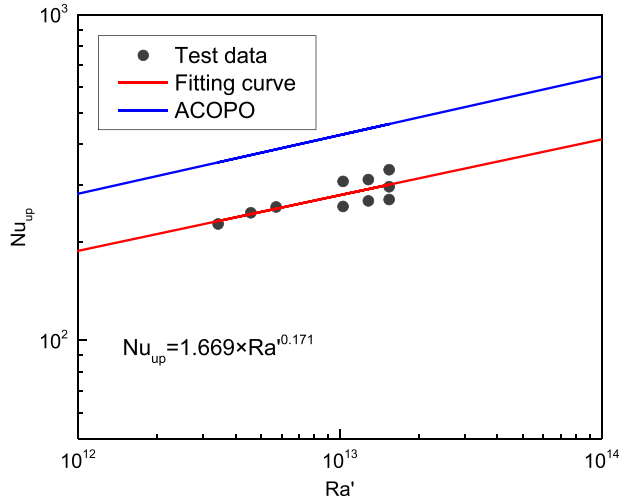

FIGURE 17
The relationship between Nu_{up} and Ra'.

partition thickness on heat transfer characteristics of two-layer molten pool under static conditions are studied, including temperature distribution characteristics, wall heat flux distribution characteristics and crust thickness distribution characteristics. Finally, the heat transfer relationship based on ellipsoidal two-layer molten pool is obtained.

The higher heating power will lead to higher temperature of molten pool, wall heat flux and thinner crust thickness. In addition, thickening the layered partition thickening, the upward thermal resistance of the lower oxide layer increases. As a result, the downward heat transfer of the molten pool increases and the crust thickness correspondingly decreases. However, the height of oxide layer has little effect on the heat transfer characteristics of two-layer molten pool with the similar volumetric power densities. Finally, the ranges of downward heat transfer Nu_{dn} and upward heat transfer Nu_{up} obtained in this paper are 106.97–211.18 and 227.62–334.12, respectively.

It should be noted that due to material limitations, the same simulant is applied to the oxide layer and metal layer, which cannot reflect the situation well in the real reactor. Therefore, more experiments need to be carried out to further analyze the heat transfer characteristics of the two-layer molten pool. Besides, CFD simulations can could be carried out to compare their results with the experiments al results. Then relevant CFD simulations of real reactors can be carried out performed, so as to provide a certain relevant reference for the IVR successful implementation of IVR.

Data availability statement

The original contributions presented in the study are included in the article/supplementary material, further inquiries can be directed to the corresponding author.

Author contributions

SW: Investigation, Methodology, Writing–original draft, Writing–review and editing. YZ: Investigation, Methodology, Supervision, Writing–review and editing. JY: Investigation, Methodology, Writing–original draft. JB: Investigation, Methodology, Writing–original draft. WT: Supervision, Writing–review and editing. SQ: Supervision, Writing–review and editing. GS: Supervision, Writing–review and editing.

Funding

The author(s) declare that no financial support was received for the research, authorship, and/or publication of this article.

Conflict of interest

The authors declare that the research was conducted in the absence of any commercial or financial relationships that could be construed as a potential conflict of interest.

Generative AI statement

The author(s) declare that no Generative AI was used in the creation of this manuscript.

Publisher's note

References

Asmolov, V., Ponomarev-Stepnoy, N. N., Strizhov, V., and Sehgal, B. R. (2001). Challenges left in the area of in-vessel melt retention. *Nucl. Eng. Des.* 209, 87–96. doi:10.1016/s0029-5493(01)00391-0

Bonnet, J. M. (1999). Thermal hydraulic phenomena in corium pools: the BALI experiment, Workshop on severe accident research held in Japan, SARJ-98.

Chen, L., Han, K., Li, T., Tian, D., Chen, Y., Chang, H., et al. (2018). Three-dimensional experiment of heat transfer for molten oxidic pool. *Prog. Nucl. Energy* 103, 209–216. doi:10.1016/j.pnucene.2017.11.014

Gaus-Liu, X., Miassoedov, A., Cron, T., and Wenz, T. (2010). In-vessel melt pool coolibility test—description and results of LIVE experiments. *Nucl. Eng. Des.* 240, 3898–3903. doi:10.1016/j.nucengdes.2010.09.001

Helle, M., Kymäläinen, O., and Tuomisto, H. (1999). "Experimental COPO II data on natural convection in homogenous and stratified pools," in *The 9th international topical meeting on nuclear reactor thermal-hydraulics (NURETH-9)*.

Henry, R. E., and Fauske, H. K. (1993). External cooling of a reactor vessel under severe accident conditions. *Nucl. Eng. Des.* 139, 31–43. doi:10.1016/0029-5493(93)90260-g

Kymäläinen, O., Tuomisto, H., Hongisto, O., and Theofanous, T. G. (1994). Heat flux distribution from a volumetrically heated pool with high Rayleigh number. *Nucl. Eng. Des.* 149, 401–408. doi:10.1016/0029-5493(94)90305-0

Luo, S., Zhang, Y., Zhou, Y., Tian, W., Su, G. H., and Qiu, S. (2018). COPRA experiment and numerical research on the behavior of internally-heated melt pool with eutectic salt. *Appl. Therm. Eng.* 140, 313–324. doi:10.1016/j.applthermaleng.2018.05.041

Ma, W. (2012). Chapter 2.6 of the book "nuclear safety in light water reactors: severe accident phenomenology".

Ma, W., Yuan, Y. R. E. B., and Sehgal, B. R. (2016). In-vessel melt retention of pressurized water reactors: historical review and future research needs. *Engineering* 2, 103–111. doi:10.1016/j.eng.2016.01.019

Miassoedov, A., Gausliu, X., Cron, T., and Fluhrer, B. (2014). "Live experiments on melt pool heat transfer in the reactor pressure vessel lower head," in International Conference on Heat Transfer, Fluid Mechanics and Thermodynamics.

Rempe, J. L., Knudson, D. L., Cebull, M., and Atwood, C. L. (1998). *Potential for In-vessel retention through Ex-vessel flooding*. Garching, Germany: Oecd/Csni Workshop on In-vessel Debris Retention and Coolability.

Rempe, J. L., Suh, K. Y., Cheung, F. B., and Kim, S. B. (2008). In-vessel retention of molten corium: lessons learned and outstanding issues. *Nucl. Technol.* 161, 210–267. doi:10.13182/nt08-a3924

Theerthan, S. A., Kolb, G., and Sehgal, B. R. (2001). Double diffusive convection in a semicircular slice with internal heat generation in one or both layers. *Exp. Heat. Transf.* 14, 283–297. doi:10.1080/089161501317098326

Theofanous, T. G., Liu, C., Additon, S., Angelini, S., Kymäläinen, O., and Salmassi, T. (1997). In-vessel coolability and retention of a core melt. *Nucl. Eng. Des.* 169, 1–48. doi:10.1016/s0029-5493(97)00009-5

Tuttle, R. M., and Becker, D. V. (2000). The Chernobyl accident and its consequences: update at the millennium. *Seminars Nucl. Med.* 30, 133–140. doi:10.1053/nm.2000.5412

Wolf, J. R., Akers, D. W., and Neimark, L. A. (1994). Relocation of molten material to the TMI-2 lower head. *Nucl. Saf.* 35, 269–279.

Younghwan, Kim, W., and Kim, M. (2013). Effect of the Fukushima nuclear disaster on global public acceptance of nuclear energy. *Energy Policy* 61, 822–828. doi:10.1016/j.enpol.2013.06.107

Zhang, L., Zhang, Y., Zhao, B., Ma, W., Zhou, Y., Su, G. H., et al. (2016a). COPRA: a large scale experiment on natural convection heat transfer in corium pools with internal heating. *Prog. Nucl. Energy* 86, 132–140. doi:10.1016/j.pnucene.2015.10.006

Zhang, L., Zhang, Y., Zhou, Y., Su, G. H., Tian, W., and Qiu, S. (2016b). COPRA experiments on natural convection heat transfer in a volumetrically heated slice pool with high Rayleigh numbers. *Ann. Nucl. Energy* 87, 81–88. doi:10.1016/j.anucene.2015.08.021

Zhang, Y. P., Su, G. H., Qiu, S. Z., Tian, W. X., Gaus-Liu, X., Kretzschmar, F., et al. (2013). A simple novel and fast computational model for the LIVE-L4. *Prog. Nucl. Energy* 68, 20–30. doi:10.1016/j.pnucene.2013.04.009

Zhou, Y., Wu, S., Zhang, Y., Yu, Z., Su, G. H., Bai, J., et al. (2020). Experimental research on heat transfer behavior of large scale two-layer salt melt pool based on COPRA facility. *Ann. Nucl. Energy* 138, 107166. doi:10.1016/j.anucene.2019.107166

10.3389/fnuen.2024.1523026

Nomenclature

H pool height (m)

L_{max} maximum arc length from bottom of ellipsoidal lower head to the contact point between layered partition and wall (m)

L_i wall arc length starting from bottom of ellipsoidal lower head (m)

Nu Nusselt number

q heat flux ($W \cdot m^{-2}$)

R pool radius (m)

T temperature (°C)

Ra' internal Rayleigh number

Greek symbols

λ thermal conductivity ($W \cdot m^{-1} \cdot K^{-1}$)

δ thickness (m)

Subscripts

ave average

dn downward

i inner

max maximum

o outer

up upper

wall wall of test section

partition layered partition